energies

MDPI

Article

Predictive Control of PV/Battery System under Load and Environmental Uncertainty

Salem Batiyah [1,2,*,†], Roshan Sharma [2,3,†], Sherif Abdelwahed [4], Waleed Alhosaini [5] and Obaid Aldosari [6,*]

[1] Department of Electrical and Electronics Engineering Technology, Yanbu Industrial College, Yanbu Industrial, Almadina 46452, Saudi Arabia
[2] Department of Electrical and Computer Engineering, Mississippi State University, Starkville, MS 39762, USA; rs2142@msstate.edu
[3] Smart Grid and Emerging Technology, Commonwealth Edison Company (ComEd), Chicago, IL 60181, USA; roshan.sharma@comed.com
[4] Department of Electrical and Computer Engineering, Virginia Commonwealth University, Richmond, VA 23284, USA; sabdelwahed@vcu.edu
[5] Department of Electrical Engineering, College of Engineering, Jouf University, Sakaka 72388, Saudi Arabia; wsalhosaini@ju.edu.sa
[6] Department of Electrical Engineering, Prince Sattam Bin Abdulaziz University, Wadi Addawaser, Najd 11991, Saudi Arabia
* Correspondence: batiyahs@rcyci.edu.sa or smb940@msstate.edu (S.B.); om.aldosari@psau.edu.sa (O.A.)
† These authors contributed equally to this work.

Abstract: The standalone microgrids with renewable energy resources (RERs) such as a photovoltaic (PV) system and fast changing loads face major challenges in terms of reliability and power management due to a lack of inherent inertial support from RERs and their intermittent nature. Thus, energy storage technologies such as battery energy storage (BES) are typically used to mitigate the power fluctuations and maintain a power balance in the system. This paper presents a model predictive control (MPC) based power management strategy (PMS) for such standalone PV/battery systems. The proposed method is equipped with an autoregressive integrated moving average (ARIMA) prediction method to forecast the load and environmental parameters. The proposed controller has the capabilities of (1) effective power management, (2) minimization of transients during disturbances, and (3) automatic switching of the operation of the PV between the maximum power point tracking (MPPT) mode and power-curtailed mode that prevents the overcharging of the battery and at the same time maximize the PV utilization. The effectiveness of the proposed method has been verified through a comprehensive simulation-based analysis.

Keywords: power management; model predictive control; dc microgrid; photovoltaic; battery energy storage

Citation: Batiyah, S.; Sharma R.; Abdelwahed S.; Alhosaini, W.; Aldosari, O. Predictive Control of PV/Battery System under Load and Environmental Uncertainty. *Energies* **2022**, *15*, 4100. https://doi.org/10.3390/en15114100

Academic Editor: Luis Hernández-Callejo

Received: 20 April 2022
Accepted: 28 May 2022
Published: 2 June 2022

1. Introduction

Recently, distributed generators (DGs) with the integration of renewable energy resources (RESs) such as photovoltaic (PV) systems have been widely considered to reduce the dependency on conventional power generation systems along with the enhancement of the quality and sustainability of the power systems [1]. Solar photovoltaic (PV) is a promising and fast-growing power generation system due to its special features such as clean energy, wide availability, technological advancement, and cost reduction. In the U.S., 17% of the total electricity is projected to come from solar by 2050 [2].

PVs alone cannot establish a self-sustaining supply system (standalone mode) due to their stochastic nature. Therefore, they are coupled with other reliable sources and/or energy storage systems (ESSs). The ESSs filter the stochastic nature by storing excess energy during over-generation and supplying energy during under-generation. The PV systems coupled together with ESSs make PV microgrid systems more flexible and reliable. Battery

energy storage (BES) is a widely adopted storage technology due to its high energy density and quick response. The BES can be used to address both the abrupt disturbances and daily profile of the PV power [3–5].

A proper power management strategy (PMS) is important in a microgrid to maintain the power balance and ensure the stability of the system. In a standalone mode, the PMS is critical due to the absence of the main grid that compensates the power disturbances originating from the environmental conditions and the load changes. When multiple sources are inter-connected, it is desired to share the power among the generators in proportion to their capacities to avoid circulating currents, over-stressing conditions, and stability issues [6]. In [7], power is shared among the sources and the storages by controlling the DC bus voltage. However, the objective of effective power management becomes a challenge if the renewable generators are operated at maximum power point (MPP), and the storage devices are in full charged/discharged conditions. This requires consideration of power-curtailment and load-shedding strategies [8]. Power-frequency droop based PMSs are used in the ac microgrid to share power among different units [9,10]. The power-frequency based droop is not feasible in the dc microgrid where frequency is absent. A centralized power management is presented in [11] for a PV/battery hybrid microgrid considering both grid-connected and islanded operation. The methods in [9–11] are based on conventional PI-based control. Though the PI controllers are easy to design and implement in linear systems, the PI design becomes complicated as the system size increases and involves highly nonlinear coupled multi input multi output (MIMO) systems with operational constraints. Model predictive control (MPC) has shown to be better at dealing with such systems.

Recently, model predictive control (MPC) has gained considerable attention and has been realized in many practical applications such as aerospace [12], electric vehicles [13], and water treatment [14]. This controller has the capability of explicitly handling complicated phenomena, such as handling multiple control objectives and actuator constraints, considering possible forecasts about time delays and disturbances in system dynamics, and responding robustly to a wide range of uncertainties.

The MPC-based controller is gaining popularity for the coordinated control of multiple converters in microgrids. MPC-based strategies are introduced to reduce the operating costs of a microgrid in [15] and to schedule power exchanges among DGs and storage in [16]. MPC-based energy management approaches are presented in [17] for hybrid wind and BES for economic BES dispatch, and in [18] for a standalone microgrid. In [19], an MPC-based control approach is employed to optimize power flow in a microgrid by maximizing the utilization of RESs and minimizing micro gas turbines. However, the aforementioned strategies are designed at the system level and ignore the structures of microgrid and power converters dynamics. In [20], a supervisory secondary control for a standalone hybrid AC/DC microgrid to adjust the set-points of RESs, BESs, and an interlinking converter has been introduced with an aim to restore the voltage and frequency near to the nominal value and reduce the total generation cost. However, the study ignores the dynamics of the RESs and their converters.

An MPC-based control strategy for the BES to smooth the PV power and stabilize the DC-bus voltage is presented in [21] without the details of the operation of the microgrid and PMS. An ultracapacitor-battery hybrid DC microgrid with MPC-based PMS is presented in [22] that utilizes ultracapacitors for fast response and battery for a slow response. However, the study considered the voltage of the DC-link as constant and ignores its dynamics. In [23], the combination of the MPC approach with the droop controller for parallel inverters in the AC microgrid is introduced. A supervisory centralized MPC strategy for the operation and power-sharing of parallel inverters is presented in [24]. In [25], an MPC-based control strategy is introduced that uses multiple buck converters and a virtual capacitor in a DC microgrid. A decentralized MPC-based controller combined with the slide-mode controller is used in [26] for multiple DGs in islanded mode to control the voltage and current under uncertainties in load parameters, unbalanced phase conditions,

and transients. However, the methods in [21–27] did not consider the intermittent nature of renewable energy resources.

An MPC-based control for bi-directional DC/DC converters and an interlinking DC/AC converter for a wind-PV-battery microgrid is introduced in [28]. An MPC-based power-sharing approach among multiple wind generators is presented in [29] without considering the storage device. The study only considers the case where the generation exceeds the load. A multi-variable MPC-based control for battery and supercapacitor converter is considered in [30] to mitigate the effect of pulsed power loads (PPL). The works in [29,30] are limited to the linearized model of the system which degrades the performance of the controller during large transients. Since MPC-based controller is flexible and can handle both linear and non-linear system models, the control technique can be utilized for power management considering the non-linear model of the system [31]. However, the study in [31] assumes that the controller has precise knowledge of the environmental and load disturbances which is practically limited. In [32], the MPC-based controller uses a non-linear model of the system along with ARIMA prediction to predict environmental and load disturbances. However, the PV operates at MPPT all the time and ignores the over/under charging scenario of the BES.

The stochastic nature of PV makes the task of power management and maintaining stability difficult in a PV microgrid system. The situation becomes more challenging in standalone systems where the main grid is absent, and minor disturbances can cause significant voltage fluctuations leading to stability issues. Continuous load changes add further complications. The main contributions of this paper are summarized as follows,

- A detailed mathematical model for the study system is developed. The model includes the complete mathematical model of the PV panels, battery system, converter dynamics and the dc bus.
- A nonlinear MPC based on the ARIMA algorithm has been proposed to effectively manage the power flow in a standalone dc microgrid with a PV-BESS-load system that has fast variations in the load and environmental conditions.
- The paper considers the various operational modes in the power management strategy such as power curtailment of the PV and proper charging/discharging of the battery. The maximum and minimum state of charge of the battery is considered to prevent it from over/under charge conditions.

The remainder of this paper is organized as follows. Section 2 describes the standalone DC microgrid study system and its mathematical model. Section 3 presents the proposed PMS. A supervisory control based on the MPC approach is developed in Section 4 to meet the PMS objectives. Simulation results for different operational modes are presented in Section 5 with concluding remarks in Section 6.

2. Study System

The study system is shown in Figure 1. It is a standalone DC microgrid that consists of a PV, a battery, and a load, all connected to a common DC bus. The PV and battery are connected to a common bus via unidirectional and bidirectional boost converters, respectively. Each DC/DC converter is controlled by the standard PWM that generates the switching signal. The detailed circuit diagram, along with the proposed control structure, is shown in Figure 2. In this study, the PV, BES and the load are residing nearby to form a DC microgrid, for example, a residential building and an electric shipboard. Therefore, the proposed controller has direct access to all the sensors, and does not require high bandwidth communication channels. However, the number of distributed proposed small entities (each entity includes a PV, a BES, and load with proposed control) can interconnect to form a larger DC microgrid. In such cases, either a centralized supervisory control can give commands to these entities or decentralized MPC-based controllers generate commands locally to achieve effective power management. The proposed method can be implemented in such cases with minor changes in the cost function. This study is focused on the development of PMS for a small scale PV-BES-load system in standalone mode.

Development of PMS for a larger system that consists of a large number of interconnected small distribution systems can be a potential future direction of the research.

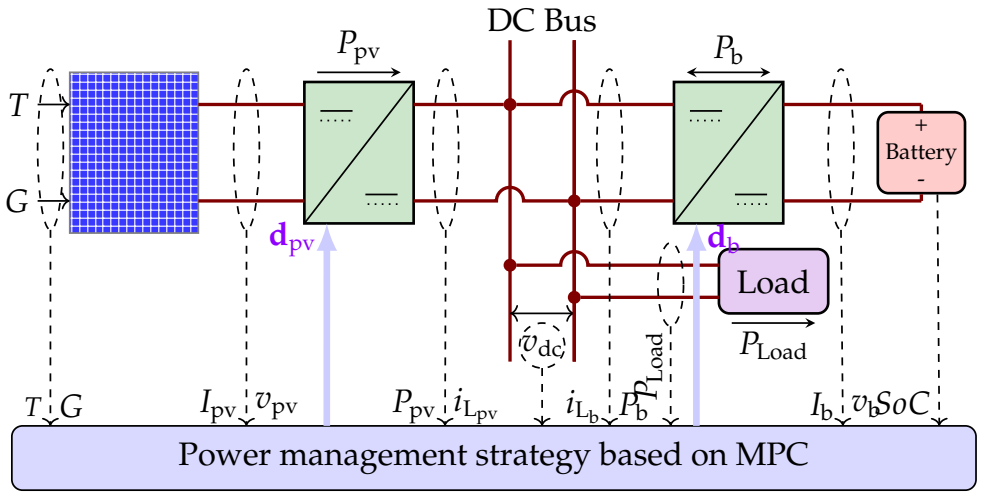

Figure 1. Power management architecture for standalone PV-battery system.

2.1. Mathematical Modeling

The mathematical model of the studied system is developed by considering the dynamic model of each subsystem.

2.1.1. Model of PV Subsystem

The nonlinear current-voltage (I-V) characteristic for a PV module [31] can be expressed as

$$I_{pv} = N_{sh} I_{ph} - N_{sh} I_o \left[\exp\left(\frac{v_{pv} + I_{pv} R_{seq}}{a N_s V_t} \right) - 1 \right] - \frac{v_{pv} + I_{pv} R_{seq}}{R_{sheq}} \tag{1}$$

where I_{pv}, I_o, I_{ph}, v_{pv}, V_t are the PV output current, the saturation current, PV current, PV voltage, and thermal voltage, respectively. The R_{seq} and R_{sheq} are the equivalent values of series and shunt resistors that are calculated as

$$R_{seq} = \frac{N_s}{N_{sh}} R_s, \qquad R_{sheq} = \frac{N_s}{N_{sh}} R_{sh} \tag{2}$$

where N_s and N_{sh} are the number of PV cells in series and parallel in a module. The parameters I_{ph}, I_o, I_{on}, and V_t depend on the temperature (T) and solar irradiance (G), and they can be expressed as follows.

$$\begin{aligned} I_{ph} &= \frac{G}{1000}(I_{SC} + k_i(T - T_n)), \\ I_o &= I_{on} \left(\frac{T}{T_n} \right)^3 \exp\left\{ \frac{q E_{gap}}{ka} \left(\frac{1}{T_n} - \frac{1}{T} \right) \right\} \\ I_{on} &= \frac{I_{SC}}{\exp\left(\frac{V_{ocn}}{a V_t N_s} \right) - 1}, \text{ and} \qquad V_t = \frac{N_s k T}{q}. \end{aligned} \tag{3}$$

In (3), I_{SC} is short circuit current, V_{ocn} is PV open circuit voltage, T_n is nominal temperature, E_{gap} is band gap energy of the semiconductor, k_i is temperature coefficient, k is boltzmann constant, q is electron charge, and a is diode ideality factor. The expression for the PV current (I_{pv}) in (1) is non-linear, and it can be solved by using Newton–Raphson method.

The dynamic equations of the PV boost converter, see Figure 2, can be derived using KVL and KCL as

$$\begin{aligned} L_{pv} \frac{d i_{L_{pv}}}{dt} &= -r_{L_{pv}} i_{L_{pv}} + v_{pv} - (1 - d_{pv}) v_{dc} \\ C_{pv} \frac{d v_{pv}}{dt} &= I_{pv} - i_{L_{pv}} \end{aligned} \tag{4}$$

where L_{pv} is the inductance of the filter, and C_{pv} is a capacitor on PV side, $i_{\mathrm{L_{pv}}}$ is filter current, and v_{dc} is the DC bus voltage. The control input is the duty cycle, $d_{\mathrm{pv}}(t) \in (0,1)$.

2.1.2. Model of Battery Energy Storage Subsystem

The BES maintains power balance in the system by proper absorption/supply of power. This absorption and supply of power alter the state-of-charge (SoC) of the BES as following

$$SoC(t) = SoC(0) - \frac{1}{3600Q}\int_0^t I_b(t)\,dt \tag{5}$$

where Q is the battery capacity in Ah, I_b is the battery current. The parameter Q is multiplied by factor 3600 in the above equation to convert its unit to SI unit as As (Ampere-seconds). For the proposed controller discussed in this paper, we have assumed that the SoC of the BES is estimated by using the method in [33] and readily available for feedback without delay.

The expression for I_b is

$$I_b = \frac{E_{bat}}{R_{bat}} - \frac{v_b}{R_{bat}} \tag{6}$$

where E_{bat}, R_{bat}, and v_b are the internal voltage, internal resistance, and the terminal voltage of the battery. The I_b is considered positive in the discharging mode, and negative in the charging mode of the BES. The term E_{bat} depends on the charging and discharging mode of operation of the battery. In this study, lithium-ion battery has been considered and its internal voltage can be written as [33,34]

$$\begin{aligned} E_{bat}^{Charge} &= E_o - K\frac{Q}{Q-i_t}i_t - K\frac{Q}{i_t-0.1Q}I_b + A\exp(-Bi_t) \\ E_{bat}^{Discharge} &= E_o - K\frac{Q}{Q-i_t}i_t - K\frac{Q}{Q-i_t}I_b + A\exp(-Bi_t) \end{aligned} \tag{7}$$

where A, B, and K are exponential voltage, exponential capacity, and polarization voltage of the battery, respectively. The term $i_t = \int_0^t I_b dt$ is the total charge flow from the battery. From (5)–(7), we get

$$\begin{aligned} E_{bat}^{Charge} &= \frac{R_{bat}(0.9-SoC)}{K+R_{bat}(0.9-SoC)}\left(E_o - K\frac{1-SoC}{SoC}Q - \frac{K}{R_{bat}(0.9-SoC)}v_b + A\exp(-BQ(1-SoC))\right) \\ E_{bat}^{Discharge} &= \frac{R_{bat}SoC}{K+R_{bat}SoC}\left(E_o - K\frac{1-SoC}{SoC}Q + \frac{K}{R_{bat}SoC}v_b + A\exp(-BQ(1-SoC))\right) \end{aligned} \tag{8}$$

From (5), the dynamics of the SoC can be re-written as

$$\frac{dSoC}{dt} = -\frac{1}{3600QR_{bat}}(E_{bat} - v_b). \tag{9}$$

By applying KVL and KCL, the dynamics of the battery converter can be written as

$$\begin{aligned} L_b\frac{di_{L_b}}{dt} &= -r_{L_b}i_{L_b} + v_b - (1-d_b)v_{dc} \\ C_b\frac{dv_b}{dt} &= I_b - i_{L_b} \end{aligned} \tag{10}$$

where $d_b(t) \in (0,1)$, and i_{L_b} are the duty cycle of BES converter, and the inductor current, respectively. The r_{L_b}, L_b are resistance and inductance of the filter; C_b is capacitor across the battery.

2.1.3. Model of the DC Bus

The DC bus voltage, v_{dc}, depends on the amount of PV power injected from the PV/BES system and power consumed by the load. The dynamics can be written by applying KCL as

$$C_{dc}\frac{dv_{dc}}{dt} = (1-d_{pv})i_{L_{pv}} + (1-d_b)i_{L_b} - \frac{v_{dc}}{R_{Load}} \tag{11}$$

where C_{dc} is a DC capacitor and R_{Load} is a DC load.

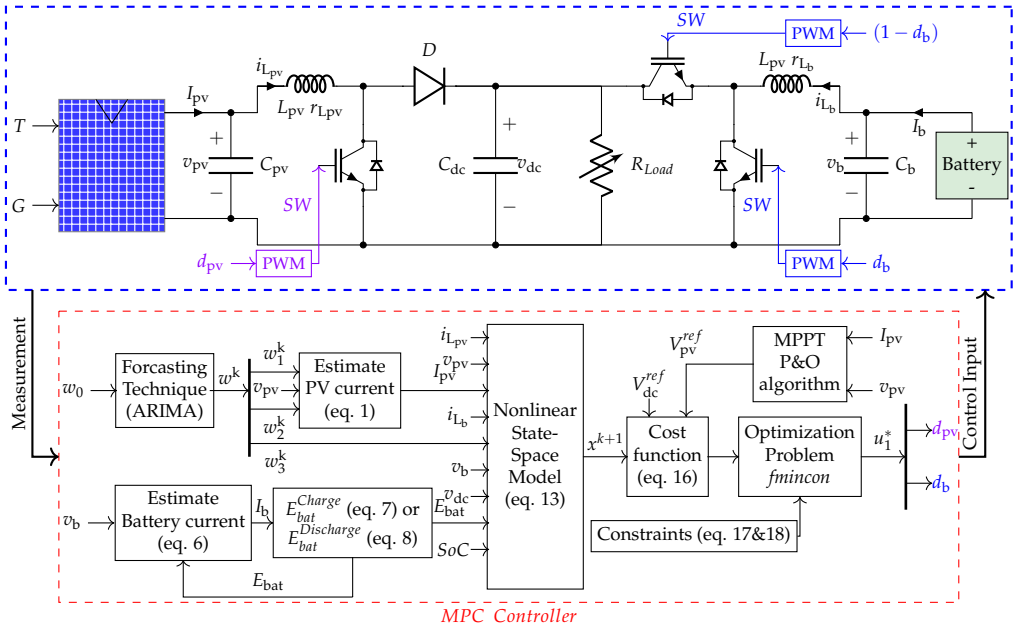

Figure 2. Circuit diagram of the PV-battery system along with MPC controller.

2.2. State Space Model of the Considered System

From (4), (9)–(11), the overall state space model of the study system of Figure 1 (details in Figure 2) is

$$\begin{aligned}
\dot{x}_1 &= \frac{1}{C_{pv}} I_{pv} - \frac{1}{C_{pv}} x_2 \\
\dot{x}_2 &= -\frac{r_{L_{pv}}}{L_{pv}} x_2 + \frac{1}{L_{pv}} x_1 - \frac{(1-u_1)}{L_{pv}} x_6 \\
\dot{x}_3 &= \frac{1}{R_{bat} C_b} (E_{bat} - x_3) - \frac{1}{C_b} x_4 \\
\dot{x}_4 &= -\frac{r_{L_b}}{L_b} x_4 + \frac{1}{L_b} x_3 - \frac{(1-u_2)}{L_b} x_6 \\
\dot{x}_5 &= -\frac{1}{3600 Q R_{bat}} (E_{bat} - x_4) \\
\dot{x}_6 &= \frac{(1-u_1)}{C_{dc}} x_2 + \frac{(1-u_2)}{C_{dc}} x_4 - \frac{1}{C_{dc} R_{Load}} x_6
\end{aligned} \tag{12}$$

where $x = [x_1, x_2, x_3, x_4, x_5, x_6]^T = [v_{pv}, i_{L_{pv}}, v_{bat}, i_{L_{bat}}, SoC, v_{dc}]^T \in \mathbb{R}^6$, $u = [u_1, u_2]^T = [d_{pv}, d_b]^T \in \mathbb{R}^2$, and $w = [w_1, w_2, w_3]^T = [T, G, R_{Load}]^T \in \mathbb{R}^3$.

3. Power Management Strategy

The PMS maintains power balance in the system, keeps the transients on DC bus voltage within the acceptable limits during disturbances, and prevents the battery from over/under charged conditions. Figure 3 shows the PMS algorithm. The proposed controller has direct access to all the system state variables, and it executes particular control actions based on the circumstances and measured data from the system.

In this study, the PV is a primary source of electricity and normally operates at MPP to maximize its utilization. The MPPT algorithm based on perturb and observe [35] is used to generate the reference bias voltage for the PV. An MPC-based voltage controller regulates the PV voltage to its reference. The battery maintains power balance by regulating the common DC bus voltage at its nominal value. However, when the battery is fully charged and the available PV power is greater than the load, the PV system cannot operate at MPP.

Under such circumstances, the battery current is set to zero to prevent it from over-charging, and the PV power is curtailed.

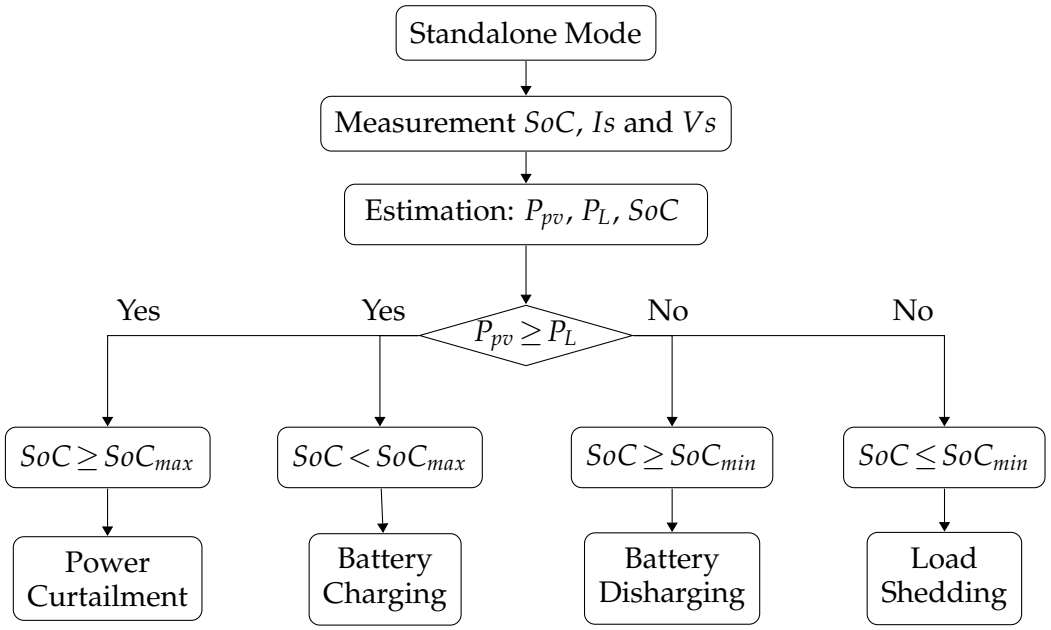

Figure 3. Power management strategy for standalone PV/battery.

Operational Modes

Based on the available PV power (P_{PV}), load demand (P_{Load}), and SoC of the BES, the following are the operational modes of the proposed PMS:

- **Mode I** ($P_{PV} > P_{Load}$ and $SoC < SoC_{max}$): In this mode, the available power from the PV is greater than the load demand, and the battery can absorb extra power. The PV operates at MPP while the battery regulates the common DC bus voltage at its nominal value.
- **Mode II** ($P_{PV} < P_{Load}$ and $SoC \geq SoC_{min}$): In this mode, the power from the PV is not enough to meet the load demand. Therefore, the battery discharges to meet the extra load. Similar to Mode I, the PV operates at MPP and the battery regulates the voltage of the DC bus.
- **Mode III** ($P_{PV} > P_{Load}$ and $SoC \geq SoC_{max}$): If the battery is fully charged and the available PV power exceeds the load demand, the battery current is set at zero to prevent it from overcharging, and the PV power is curtailed. The power curtailment is achieved by operating the PV to regulate the DC bus voltage at its nominal value.
- **Mode IV** ($P_{PV} = 0$ and $SoC \geq SoC_{min}$): During cloudy days and at night, the PV power is not available. The PV, in this mode, is disconnected, and the battery regulates DC bus voltage to meet the load demand.

Whenever $P_{PV} < P_{Load}$ and $SoC \leq SoC_{min}$, the battery should cease the supply of power and the extra non-critical load should be disconnected from the system. The load-shedding mode of operation is beyond the scope of this paper.

4. The Proposed MPC-Based Control Method

4.1. Model Predictive Control Approach

The proposed control is based on the MPC approach, which is shown in Figure 4. For each time instance, the MPC uses feedback from the actual plant as initial states and solves the dynamic model of the system to predict future states. Based on these predicted states and the desired trajectories, the control sequence is generated over a given horizon by solving an optimization problem. As a part of the optimization problem, a cost function is defined based on the desired behavior of the system, forecasted disturbances, and system

constraints. Once the optimization problem is solved, only the first obtained control signals from the control sequence are applied to the system.

For the purpose of the control and the prediction, the continuous-time dynamic model described in (12) can be discretized using a forward Euler method as

$$x(k+1) = f(x(k), u(k), \omega(k)), \qquad x(0) = x_0 \tag{13}$$

where k, $x(k)$, $u(k)$, and $\omega(k)$ represent sample step, state variables, control inputs, and environmental parameters, respectively. The chosen sampling time should be small enough to observe the nonlinearity in the system model, but large enough to avoid computation burden.

The MPC-based controller solves the dynamic model to predict the future behavior of the system. The temperature, solar irradiance, and the load variation are part of the system dynamics that have a significant impact on the control performance. Therefore, the controller requires the future values of these non-deterministic parameters. A suitable forecasting technique that utilizes the historical and currently measured signals can be used to estimate the future values of these parameters which are then used in solving the dynamic model. The optimization is then performed on the basis of the estimated disturbances and the currently measurement system states over a given time horizon. This paper incorporates ARIMA prediction [36] along with the proposed MPC-based controller.

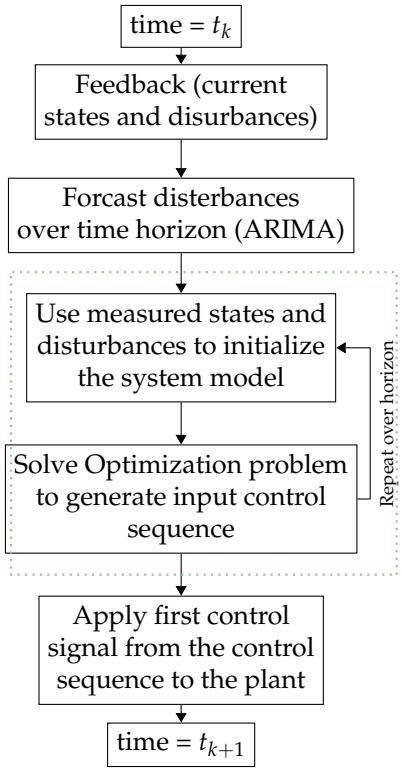

Figure 4. Proposed MPC based on PMS.

4.2. Control Problem Formulation

The mathematical model of the studied system of Figure 2 is derived in Section 2. The duty cycles, d_{pv} and d_b, of the DC/DC converters act as control inputs. The objective of the MPC controller is to maintain the DC bus voltage at its nominal value and perform the MPPT of the PV during normal operation. The optimization problem can be formulated as

$$\min_{u(\cdot)\in\mathbb{R}^m} J(x(\cdot), u(\cdot)) = \min_{u(\cdot)\in\mathbb{R}^m} \sum_{k=0}^{N-1} L(x(k), u(k)) \tag{14}$$

where $J(x(\cdot), u(\cdot))$ is a cost function. The function $L(\cdot)$ is

$$L(x(k), u(k)) = F\left\| V_{dc}^{ref} - v_{dc}(k) \right\| + Q\alpha \left\| I_{L_b} \right\| + P(1-\alpha)\left\| V_{pv}^{ref} - v_{pv}(k) \right\| + \sum_{i=1}^{2} R_i \|\Delta u_i\| \tag{15}$$

subject to

$$\begin{aligned} &x(k+1) = f(x(k), u(k), \omega(k)) \quad \forall k \in [0, .., N-1] \\ &SoC_{min} \leq SoC \leq SoC_{max} \\ &u_i^{min} \leq u_i \leq u_i^{max}. \end{aligned} \tag{16}$$

In this optimization problem, V_{dc}^{ref} is the reference value of the DC bus, and V_{pv}^{ref} is the reference PV voltage obtained from the MPPT algorithm. The parameters, F, P, R, and Q are the weighting factors for each term in the cost function. The parameter α is set at zero in normal operation (Mode I & II), and it is set at one in Mode III operation. In the cost function of (15), the first term regulates the DC bus voltage at its reference value. The second term is activated only in Mode III that sets BES current to zero. The third term is activated only in Mode I and II operation ($\alpha = 0$) that operates PV at MPP. The fourth term minimizes the variation of the control input.

The system constraints in the optimization problem are the system dynamic equations, the limits on the battery SoC, and the limits on the control inputs. In this paper, the minimum and the maximum values of SoC are defined as 20% and 90%, respectively. Since, the control inputs, u_is, are the duty cycles of PV and battery converter, their values should be within the range of zero and one. The above optimization problem can be solved directly using the *fmincon* solver in MATLAB.

5. Simulation Results

Figure 2 shows the complete schematic circuit diagram of the study system, along with the proposed controller. The microgrid consists of a PV system with a rated power of 9.5 kW, a lithium-ion battery system of 20 Ah capacity, and varying load. The nominal DC bus voltage is $V_{dc}^{ref} = 600$ V. The system parameters are shown in Table 1.

Table 1. System Parameters.

Parameter	Symbol	Value
PV Capacitor	C_{pv}	300 µF
PV Inductor	L_{pv}	10 mH
Resistance of Inductance	$r_{L_{pv}}$	10 mΩ
Battery Capacitor	C_b	300 µF
Battery Inductor	L_b	10 mH
Resistance of Inductance	r_{L_b}	10 mΩ
DC bus Capacitor	C_{dc}	1500 µF
Switch Frequency	f_{sw}	10 kHz
PV Parameters		
Maximum Power	MP	213.15 W
MP, OC Voltage	V_{MP}, V_{oc}	29 V, 36.3 V
SC, MP Current	I_{sc}, I_{MP}	7.84 A, 7.35 A
battery parameters		
Battery Voltage	V_b	300 V
Battery Capacity	Q	20 Ah

The simulation of the study system was conducted in the Matlab platform to verify the performance of the proposed control strategy. The sample time (T_s) is 10 µs, the control interval time (t_c) is 10 ms, and the prediction horizon is one. The nonlinear optimization problem formulated in Section 4 is solved in Matlab using *fmincon* solver. In this simulation study, the weighting factors, F, P, R and Q, in the cost function are 0.75, 0.15, 0.1, and 0.15, respectively. The responses of the proposed system and their performances are studied for varying environmental and load conditions.

5.1. Mode I Operation

Figure 5 shows the response of the system in Mode I operation where the available PV power is larger than the load demand, and the battery *SoC* is below its maximum limit. Therefore, the battery absorbs extra power from the system and maintains power balance in the system. Initially, the load demand is slightly greater than the available power, see Figure 5. The battery discharges to provide the deficit power and regulates DC bus voltage at 600 V. At $t = 4$ s, due to the changes in the environmental parameters and the load demand, the load falls below the available PV power. The PV continues to operate at MPP, and the battery absorbs the extra power to maintain a power balance in the system. The system with the proposed MPC-based PMS has smooth transients during the disturbances.

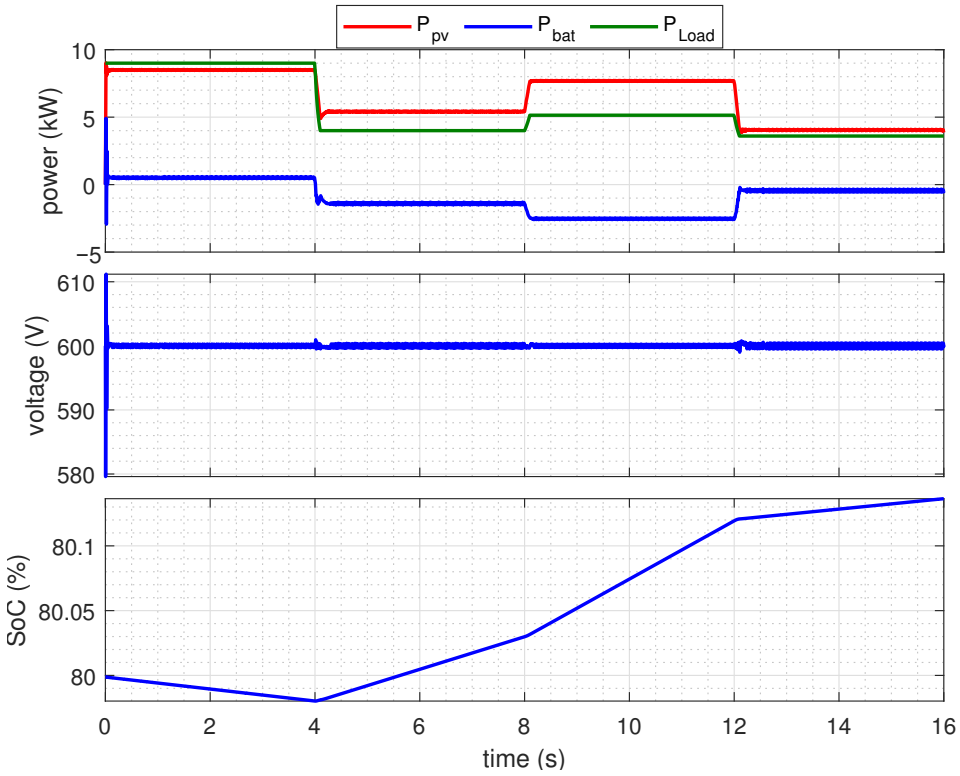

Figure 5. Response of the proposed system in Mode I operation.

5.2. Mode II Operation

The response of the system in Mode II operation is shown in Figure 6. Initially, the available PV power is greater than the load demand. Therefore, the battery absorbs extra power from the system and regulates DC bus voltage at 600 V. At $t = 4$ s, due to the changes in the environmental parameters and the load demand, the load demand exceeds the available PV power and the *SoC* of the battery is above its minimum limit. Therefore, the PV continues to operate at MPP, and the battery provides the deficit power to meet the load demand. The DC bus voltage is regulated at 600 V with smooth transients during system disturbances.

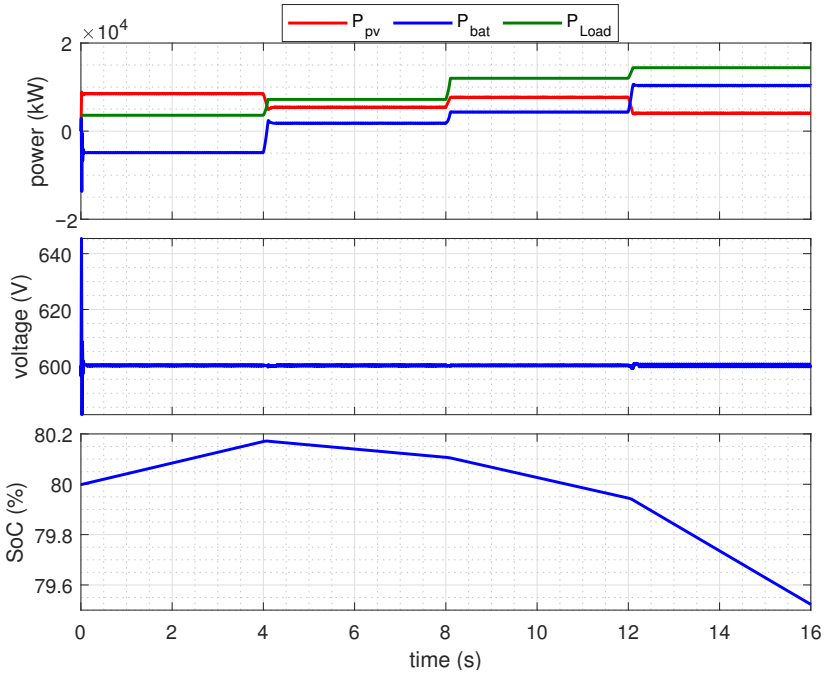

Figure 6. Response of the proposed system in Mode II operation.

5.3. Mode III Operation

The response of the proposed system in the Mode III operation is shown in Figure 7. The load demand is initially less than the power generated by PV system, and the battery absorbs the extra power. At $t = 4.2$ s, the *SoC* of the BES reaches its upper limit (90%). Therefore, the battery stops absorbing power from the DC bus, and the power from the PV is curtailed to maintain DC bus voltage at 600 V. At $t = 12.2$ s, the load demand is above the available PV power. Therefore, the PV operation is switched to MPPT mode, and the battery discharges to supply the extra load demand. Figure 7 shows that the system with proposed control responds to the disturbances with smooth transients between the power-curtailment mode and MPPT mode.

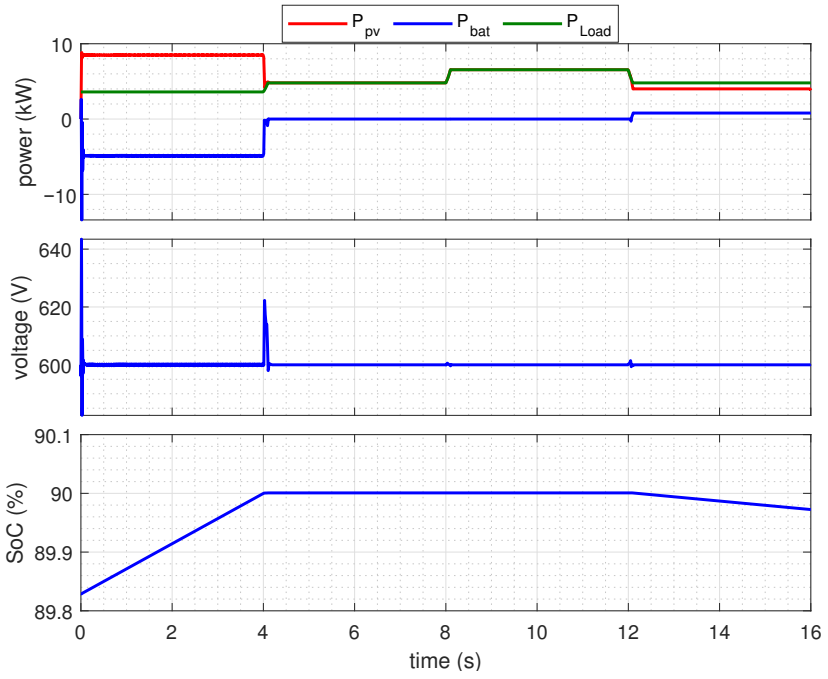

Figure 7. Response of the proposed system in Mode III operation.

5.4. Mode IV Operation

Figure 8 shows the Mode IV operation of the proposed system. Initially, the PV power is slightly greater than the load demand, and the *SoC* of the battery is below 90%. Therefore, the battery absorbs extra power. At $t = 4.2$ s, the PV power drops to zero. Since the battery *SoC* is above its lower limit, the BES supplies total power to meet the load demand.

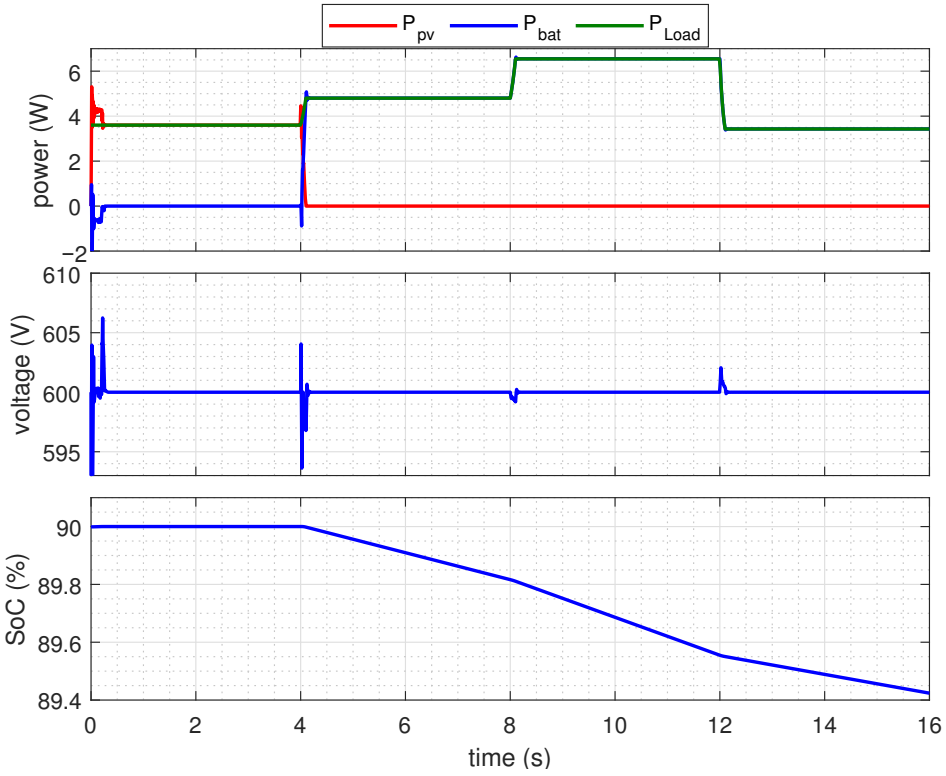

Figure 8. Response of the proposed system in Mode IV operation.

5.5. Comparison of the Proposed Controller with PI Controller

In this section, the performance of the proposed control is compared with the PI controller of [7]. The gains of the PI for the study system of Figure 2 are designed optimally using the linear quadratic regulator (LQR) technique [37]. The PV operates at MPP, and the battery regulates the DC bus voltage at 600 V. The PV and battery controllers can be treated independently and the control gains are designed separately. The PV system and the battery control gains are $k_1^{pv} = -1000$, $k_2^{pv} = -21.3$, $k_3^{pv} = 1.7$, $k_1^b = 13{,}300$, $k_2^b = -16$, $k_3^b = -42.2$, and $k_4^b = 0.223$.

Figures 9 and 10 show the response of the considered system with the proposed MPC and the PI control to the same disturbances. At $t = 1$ s, the irradiance increases from 500 to 1000 W/m^2, the temperature reduces from 35 °C to 25 °C, and the load remains at 7.2 kW. At $t = 2$ s, the load rises to 14.4 kW. The results show that both control methods regulate the DC bus voltage at 600 V. However, the proposed MPC has smoother transients, see Figure 9. Moreover, the deviation of the DC voltage from its nominal value is quantified using the voltage regulation index (VRI) which is defined as $VRI\ \% = \left\| \frac{v_{dc} - V_{dc}^{ref}}{V_{dc}^{ref}} \right\| \times 100$. Figure 10 shows that the proposed MPC-based control approach has low voltage deviation and better control over the DC bus voltage. The average error in DC bus voltage is 0.001356 for proposed MPC and 0.011267 for conventional PI control.

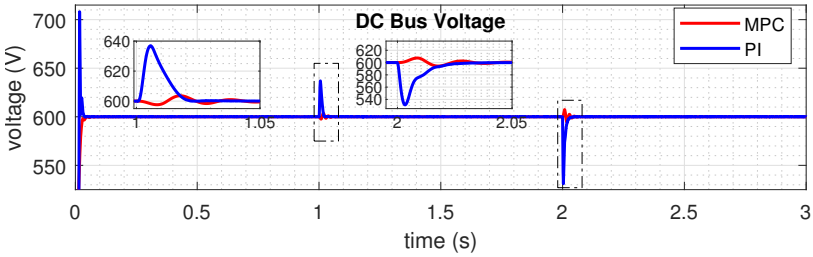

Figure 9. Response of DC bus voltage with proposed MPC and PI control.

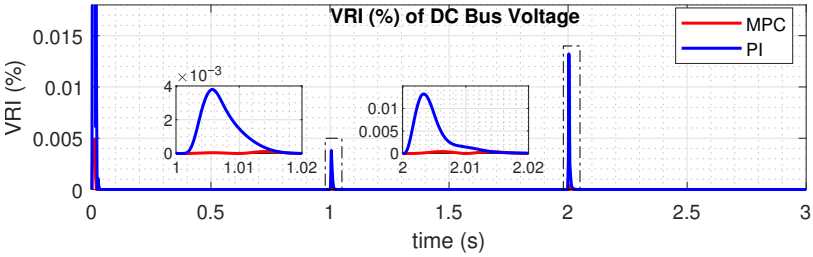

Figure 10. Voltage regulation index (VRI) of DC bus voltage for MPC and PI.

5.6. Response of the Proposed Control to the Real-World Environmental and Load Profile

Figure 11 shows the 24-h load, temperature, and irradiance profile. The solar irradiance and temperature were measured at Lowery Range Solar Station in Colorado, USA, on 13 August 2013 [38], and the load profile is obtained and modified for residential and commercial consumers [39]. For the simulation study, the 24-h profile has been scaled down to 300 s. Figure 12 shows the response of the DC bus voltage. The PV power and the battery power profiles are shown in Figure 13. Figure 14 shows the SoC of the battery. It is observed that the proposed MPC control effectively regulates the DC bus voltage at the desired level of 600 V and manages the power balance in the system. During the daytime (here between $t = 30$ s and $t = 120$ s), the PV power generation exceeds the load demand, and the battery absorbs extra power. In the morning (before $t = 30$ s) and in the late afternoon (after $t = 120$ s), the PV and the battery supply the power to meet the load demand.

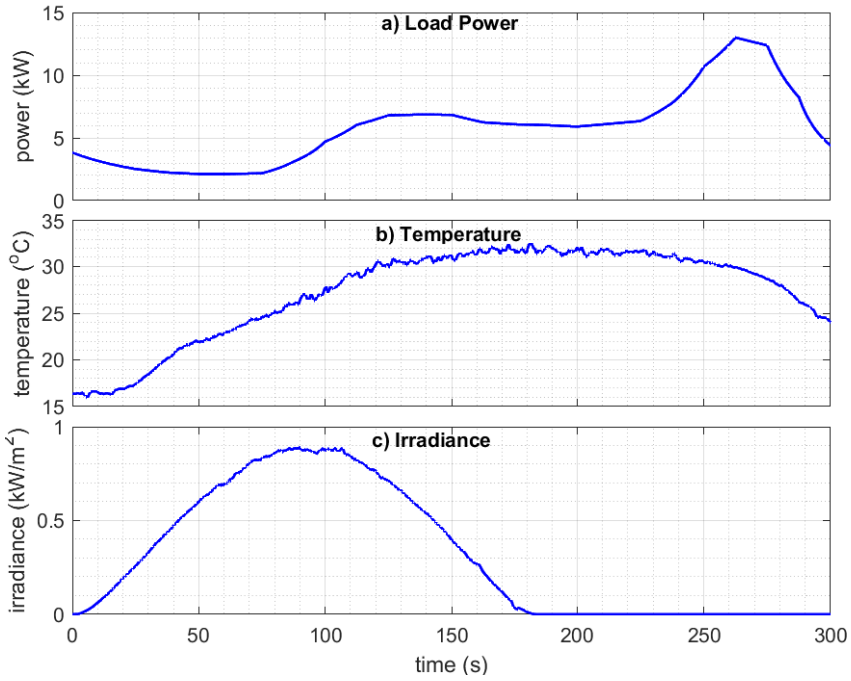

Figure 11. Real-world disturbances profile: (**a**) Load Demand, (**b**) temperature, (**c**) solar irradiance.

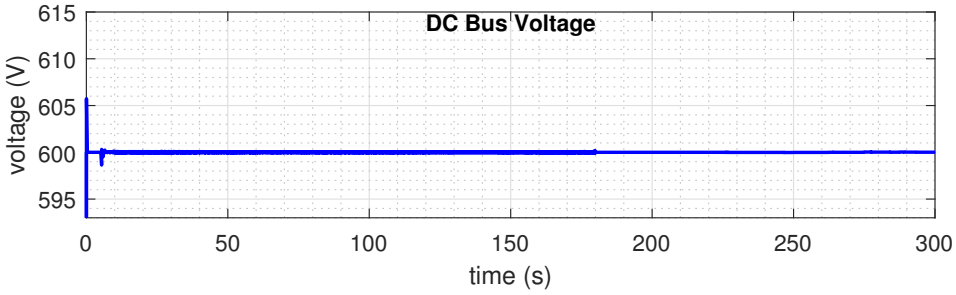

Figure 12. DC bus voltage in response to the real-world disturbances data.

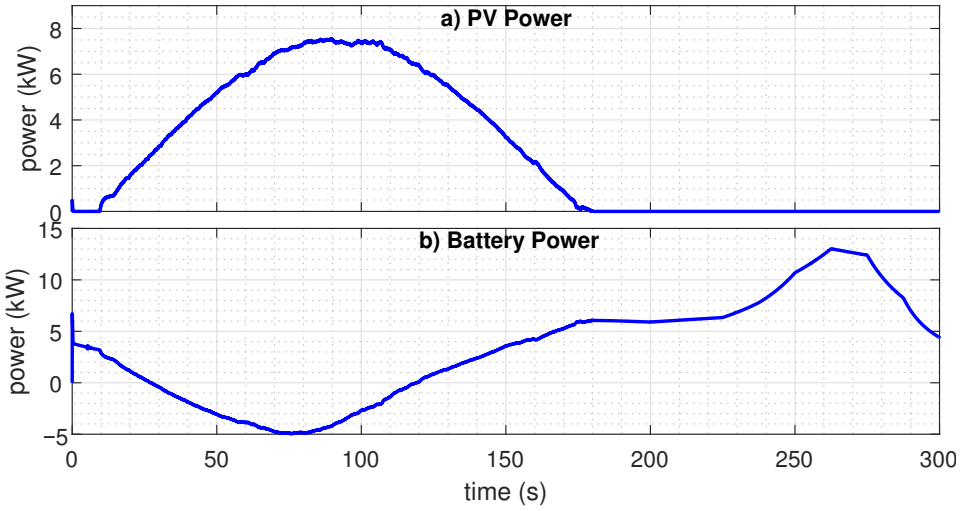

Figure 13. PV and battery power in response to the real-world disturbances data.

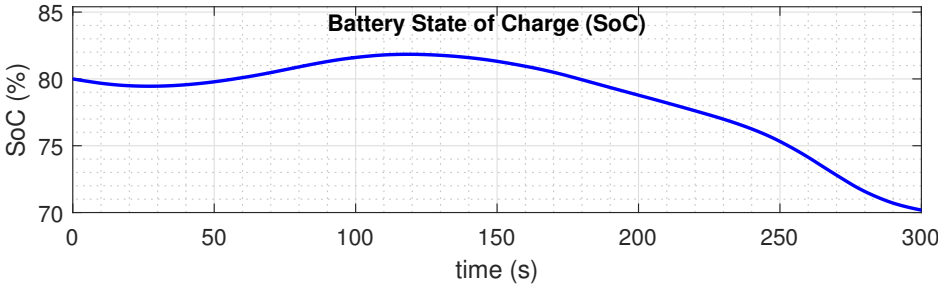

Figure 14. Battery SOC in response to the real-world disturbances data.

6. Conclusions

This paper presents a model predictive control (MPC) approach for the power management in a DC microgrid system with a PV generator, a load, and a battery. The proposed controller manages power balance by operating PV at maximum power point (MPP) and controlling the battery to regulate the common DC bus voltage. However, when the available PV power exceeds the load and the battery is fully charged, the proposed controller smartly sets the battery current to zero and operates the PV at power-curtailed mode. The proposed PMS effectively deploys the PV and battery to meet the load demand. The ARIMA prediction method is incorporated in the proposed MPC to forecast the environment and load variations. The effectiveness of the proposed controller has been verified through extensive simulation, a comparative study with PI control approach, and system responses to real-world environmental and load disturbances. Consequently, this paper can be extended to develop PMS in such a larger microgrid with many distributed entities, which can be considered for the future direction of this research.

Author Contributions: Conceptualization, S.B., R.S. and O.A.; Investigation, O.A.; Methodology, S.B., R.S. and O.A.; Software, S.B.; Supervision, S.A.; Validation, W.A.; Writing—original draft, S.B. and R.S.; Writing—review & editing, S.A., W.A. and O.A. All authors have read and agreed to the published version of the manuscript.

Funding: This publication was supported by the Deanship of Scientific Research at Prince Sattam bin Abdulaziz University, Alkharj, Saudi Arabia under the research project 2021/01/18739.

Institutional Review Board Statement: Not applicable.

Informed Consent Statement: Not applicable.

Data Availability Statement: Not applicable.

Conflicts of Interest: The authors declare no conflict of interest.

References

1. Zia, M.F.; Benbouzid, M.; Elbouchikhi, E.; Muyeen, S.M.; Techato, K.; Guerrero, J.M. Microgrid Transactive Energy: Review, Architectures, Distributed Ledger Technologies, and Market Analysis. *IEEE Access* **2020**, *8*, 19410–19432. [CrossRef]
2. Annual Energy Outlook 2020 with Projections to 2050. 2020. Available online: https://www.eia.gov/outlooks/aeo/pdf/aeo2020.pdf (accessed on 19 April 2022).
3. Qunais, T.; Sharma, R.; Karimi-Ghartemani, M.; Silwal, S.; Khajehoddin, S.A. Application of Battery Storage System to Improve Transient Responses in a Distribution Grid. In Proceedings of the 2019 IEEE 28th International Symposium on Industrial Electronics (ISIE), Vancouver, BC, Canada, 12–14 June 2019; pp. 52–57. [CrossRef]
4. Sharma, R.; Karimi-Ghartemani, M. Addressing Abrupt PV Disturbances, and Mitigating Net Load Profile's Ramp and Peak Demands, Using Distributed Storage Devices. *Energies* **2020**, *13*, 1024. [CrossRef]
5. Sharma, R.; Zakerian, A.; Karimi-Ghartemani, M. Local Controller for an Autonomous Grid-Supportive Battery Energy Storage System. *IEEE Trans. Power Electron.* **2021**, *37*, 2191–2202. [CrossRef]
6. Nejabatkhah, F.; Li, Y.W. Overview of Power Management Strategies of Hybrid AC/DC Microgrid. *IEEE Trans. Power Electron.* **2015**, *30*, 7072–7089. [CrossRef]
7. Merabet, A.; Ahmed, K.T.; Ibrahim, H.; Beguenane, R.; Ghias, A.M. Energy management and control system for laboratory scale microgrid based wind-PV-battery. *IEEE Trans. Sustain. Energy* **2017**, *8*, 145–154. [CrossRef]
8. Cai, H.; Xiang, J.; Wei, W. Decentralized Coordination Control of Multiple Photovoltaic Sources for DC Bus Voltage Regulating and Power Sharing. *IEEE Trans. Ind. Electron.* **2018**, *65*, 5601–5610. [CrossRef]
9. Mahmood, H.; Jiang, J. Decentralized Power Management of Multiple PV, Battery, and Droop Units in an Islanded Microgrid. *IEEE Trans. Smart Grid* **2019**, *10*, 1898–1906. [CrossRef]
10. Karimi, Y.; Guerrero, J.M.; Oraee, H. Decentralized method for load sharing and power management in a hybrid single/three-phase islanded microgrid consisting of hybrid source PV/battery units. In Proceedings of the 2016 IEEE Energy Conversion Congress and Exposition (ECCE), Milwaukee, WI, USA, 18–22 September 2016; pp. 1–8. [CrossRef]
11. Yi, Z.; Dong, W.; Etemadi, A.H. A Unified Control and Power Management Scheme for PV-Battery-Based Hybrid Microgrids for Both Grid-Connected and Islanded Modes. *IEEE Trans. Smart Grid* **2018**, *9*, 5975–5985. [CrossRef]
12. Bayat, F. Model Predictive Sliding Control for Finite-Time Three-Axis Spacecraft Attitude Tracking. *IEEE Trans. Ind. Electron.* **2019**, *66*, 7986–7996. [CrossRef]
13. He, H.; Jia, H.; Sun, C.; Sun, F. Stochastic Model Predictive Control of Air Conditioning System for Electric Vehicles: Sensitivity Study, Comparison, and Improvement. *IEEE Trans. Ind. Inform.* **2018**, *14*, 4179–4189. [CrossRef]
14. Wang, D.; Xiang, H. Composite Control of Post-Chlorine Dosage During Drinking Water Treatment. *IEEE Access* **2019**, *7*, 27893–27898. [CrossRef]
15. Parisio, A.; Rikos, E.; Glielmo, L. A Model Predictive Control Approach to Microgrid Operation Optimization. *IEEE Trans. Control. Syst. Technol.* **2014**, *22*, 1813–1827. [CrossRef]
16. Ouammi, A.; Dagdougui, H.; Dessaint, L.; Sacile, R. Coordinated Model Predictive-Based Power Flows Control in a Cooperative Network of Smart Microgrids. *IEEE Trans. Smart Grid* **2015**, *6*, 2233–2244. [CrossRef]
17. Abdeltawab, H.H.; Mohamed, Y.A.I. Market-Oriented Energy Management of a Hybrid Wind-Battery Energy Storage System Via Model Predictive Control With Constraint Optimizer. *IEEE Trans. Ind. Electron.* **2015**, *62*, 6658–6670. [CrossRef]
18. Minchala-Avila, L.I.; Garza-Castañon, L.; Zhang, Y.; Ferrer, H.J.A. Optimal Energy Management for Stable Operation of an Islanded Microgrid. *IEEE Trans. Ind. Inform.* **2016**, *12*, 1361–1370. [CrossRef]
19. Hooshmand, A.; Malki, H.A.; Mohammadpour, J. Power flow management of microgrid networks using model predictive control. *Comput. Math. Appl.* **2012**, *64*, 869–876. [CrossRef]
20. Lee, J.; Kim, Y.; Moon, S. Novel Supervisory Control Method for Islanded Droop-Based AC/DC Microgrids. *IEEE Trans. Power Syst.* **2019**, *34*, 2140–2151. [CrossRef]
21. Lei, M.; Yang, Z.; Wang, Y.; Xu, H.; Meng, L.; Vasquez, J.C.; Guerrero, J.M. An MPC-Based ESS Control Method for PV Power Smoothing Applications. *IEEE Trans. Power Electron.* **2018**, *33*, 2136–2144. [CrossRef]

22. Hredzak, B.; Agelidis, V.G.; Jang, M. A model predictive control system for a hybrid battery-ultracapacitor power source. *IEEE Trans. Power Electron.* **2014**, *29*, 1469–1479. [CrossRef]
23. Dragičević, T. Model Predictive Control of Power Converters for Robust and Fast Operation of AC Microgrids. *IEEE Trans. Power Electron.* **2018**, *33*, 6304–6317. [CrossRef]
24. Tan, K.; So, P.; Chu, Y.; Chen, M. Coordinated control and energy management of distributed generation inverters in a microgrid. *IEEE Trans. Power Deliv.* **2013**, *28*, 704–713. [CrossRef]
25. Yi, Z.; Zhao, X.; Shi, D.; Duan, J.; Xiang, Y.; Wang, Z. Accurate Power Sharing and Synthetic Inertia Control for DC Building Microgrids With Guaranteed Performance. *IEEE Access* **2019**, *7*, 63698–63708. [CrossRef]
26. Tavakoli, A.; Negnevitsky, M.; Muttaqi, K.M. A decentralized model predictive control for operation of multiple distributed generators in an islanded mode. *IEEE Trans. Ind. Appl.* **2017**, *53*, 1466–1475. [CrossRef]
27. Tan, K.; Peng, X.; So, P.L.; Chu, Y.C.; Chen, M. Centralized control for parallel operation of distributed generation inverters in microgrids. *IEEE Trans. Smart Grid* **2012**, *3*, 1977–1987. [CrossRef]
28. Shan, Y.; Hu, J.; Chan, K.W.; Fu, Q.; Guerrero, J.M. Model Predictive Control of Bidirectional DC-DC Converters and AC/DC Interlinking Converters-A New Control Method for PV-Wind-Battery Microgrids. *IEEE Trans. Sustain. Energy* **2018**, *10*, 1823–1833. [CrossRef]
29. Kou, P.; Liang, D.; Wang, J.; Gao, L. Stable and Optimal Load Sharing of Multiple PMSGs in an Islanded DC Microgrid. *IEEE Trans. Energy Convers.* **2018**, *33*, 260–271. [CrossRef]
30. Mardani, M.M.; Khooban, M.H.; Masoudian, A.; Dragičević, T. Model Predictive Control of DC–DC Converters to Mitigate the Effects of Pulsed Power Loads in Naval DC Microgrids. *IEEE Trans. Ind. Electron.* **2019**, *66*, 5676–5685. [CrossRef]
31. Batiyah, S.; Zohrabi, N.; Abdelwahed, S.; Sharma, R. An MPC-Based Power Management of a PV/Battery System in an Islanded DC Microgrid. In Proceedings of the 2018 IEEE Transportation Electrification Conference and Expo (ITEC), Long Beach, CA, USA, 13–15 June 2018; pp. 231–236.
32. Batiyah, S.; Sharma, R.; Abdelwahed, S.; Zohrabi, N. An MPC-based power management of standalone DC microgrid with energy storage. *Int. J. Electr. Power Energy Syst.* **2020**, *120*, 105949. [CrossRef]
33. Motapon, S.N.; Lupien-Bedard, A.; Dessaint, L.; Fortin-Blanchette, H.; Al-Haddad, K. A Generic Electrothermal Li-ion Battery Model for Rapid Evaluation of Cell Temperature Temporal Evolution. *IEEE Trans. Ind. Electron.* **2017**, *64*, 998–1008. [CrossRef]
34. Tremblay, O.; Dessaint, L.A. Experimental validation of a battery dynamic model for EV applications. *World Electr. Veh. J.* **2009**, *3*, 289–298. [CrossRef]
35. Li, X.; Wang, Q.; Wen, H.; Xiao, W. Comprehensive Studies on Operational Principles for Maximum Power Point Tracking in Photovoltaic Systems. *IEEE Access* **2019**, *7*, 121407–121420. [CrossRef]
36. Yunus, K.; Thiringer, T.; Chen, P. ARIMA-Based Frequency-Decomposed Modeling of Wind Speed Time Series. *IEEE Trans. Power Syst.* **2016**, *31*, 2546–2556. [CrossRef]
37. Karimi-Ghartemani, M.; Khajehoddin, S.A.; Jain, P.; Bakhshai, A. Linear quadratic output tracking and disturbance rejection. *Int. J. Control* **2011**, *84*, 1442–1449. [CrossRef]
38. Yoder, M.; Andreas, A. *Lowry Range Solar Station: Arapahoe County, Colorado (Data)*; National Renewable Energy Laboratory: Golden, CO, USA, 2014.
39. Li, X. *Microgrid Load and LCOE Modelling Results*; National Renewable Energy Laboratory: Golden, CO, USA, 2018.